Polarization of Muons in Cooling Channel

A. Van Ginneken
Fermi National Accelerator Laboratory*
P. O. Box 500, Batavia, IL 60510

August 8, 2000

Abstract

Polarization of muons in the cooling channel is investigated in the spirit of an earlier similar study for the decay channel. Algorithms to transport polarized muons through absorbers are presented. Care is taken to preserve correlations between polarization and phase space variables. Some examples are included by way of illustration.

1 Introduction

Transport of polarized muons through the *cooling channel* leading to a muon collider or storage ring is investigated with the Monte Carlo code SIMUCOOL which is upgraded to include effects of polarization. In [1] changes in polarization in the *decay channel* are studied. The Monte Carlo procedure attaches a spin vector to each muon acquired when the pion parent decays, then follows the evolution of this spin vector as the muon traverses the decay channel. Transport of spin through absorbers is added in the present study but all simplifying assumptions used in [1] are retained in traversing the solenoids and cavities which link the absorbers in the cooling channel: g=2, with idealized fields which are constant and point along the z-axis. Transport of spin through arbitrary fields is deferred to a later installment.

The procedure of simulating large angle scatterings as individual events while combining all those below some suitably chosen threshold into a multiple scattering distribution as advocated in [2] is well suited to inclusion

*Work supported by the U.S. Department of Energy under contract No. DE-AC02-76CHO3000.

of polarization because '... polarization effects are proportionately more affected by the few scatterings at large angles than is the angular distribution itself ...' [3]. In an absorber, therefore, correlations are expected to develop between transverse phase space variables and polarization mostly as a result of relatively few large angle scatterings and by simulating these individually such correlations are included explicitly.

In [4] a procedure is presented for keeping track of energy loss and angular dispersion of charged particles—along with their correlation—in a thick target. This procedure entails fixing a threshold below which the muon's angular deflections are chosen from an Edgeworth series (which improves upon the usual Gaussian approximation) while above it full two-body μ-nucleus-collisions are simulated. Angular deflections associated with μe^- collisions are rather small compared with those incurred in $\mu-$nuclear scattering and are estimated based on a Gaussian approximation. This procedure, along with a similar treatment of energy loss fluctuations has now been implemented into SIMUCOOL and can be utilized for tracking particles through thick targets. To include polarization in the above scheme for tracking muons through a cooling channel, one needs algorithms to simulate change in helicity due to single encounters (above threshold) as well as to treat the change due to a large number of encounters (below threshold), while transport of spin through magnets and cavities may be taken from [1].

Below, in Sec. 2, the physical basis and Monte Carlo implementation of these algorithms are briefly described and in Sec. 3 this is applied to some examples. Concluding remarks are in Sec. 4.

2 Polarization

In general, SIMUCOOL tracks the muons step-wise through the geometry. This is always done when traversing an absorber but elsewhere—where possible—advantage is taken of analytical short-cuts. Thus, when a solenoid is assumed to have an ideal field with $\vec{B} = B_z\hat{z}$, the muon orbit is easily described and given its coordinates and momenta at the entrance of the magnet, those at the exit are readily determined along with aperture checking during transit. To avoid dealing with end fields the entire channel is assumed to be enveloped by a solenoid. While this may be impractical as well as cause the beam to acquire an undesired net angular momentum, it is nonetheless a good first approximation to study depolarization in a cooling channel. Cavities are assumed to have zero extent and to deliver a finite energy kick to the muon. For an electric field with $\vec{E} = E_z\hat{z}$ (varying sinu-

soidally in time) this kick corresponds to a change in momentum along p_z only, with p_x and p_y left unchanged. The algorithms for changes in polarization resulting from traversing solenoids, cavities and absorbers are now examined.

2.1 Solenoids and Cavities

Using the above analytical shortcuts it is found in [1] that for transport through solenoids and cavities it is easiest to keep track of the muon spin four-vector, s, *in the lab frame*. But expressions for changes in polarization in an absorber, due to Coulomb scattering, are generally stated in terms of the spin vector, $\hat{\zeta}$, in the muon *rest frame*—where $|\hat{\zeta}| = 1$ and the fourth component vanishes. A simple way out is to use each approach in its own domain and convert the three-vector part of s to $\hat{\zeta}$ via the Lorentz boost:

$$\hat{\zeta} = \vec{s} - \vec{p}\frac{\vec{p}\cdot\vec{s}}{\varepsilon(\varepsilon+m)} \tag{1}$$

where $\vec{p}$ and ε are the muon momentum and total energy in the lab.

2.2 Absorbers

Polarization change in an absorber starts with polarization change in a single scattering. As in [4] a *projected* angle threshold, θ_c, is introduced, above which events are to be simulated individually. To be precise: for an event to qualify for this treatment, it is sufficient that *either* projected angle, θ_x or θ_y, is larger than θ_c. Conversely, only when both θ_x and θ_y are below θ_c is the event included collectively in the multiple scattering. The algorithms for calculating polarization changes in single and for multiple scattering are discussed below.

2.2.1 Single Scattering

The polarization change in single muon-nuclear scattering is written as [5]

$$P' = P\left[1 - \frac{2\sin^2(\theta/2)}{\gamma^2\cos^2(\theta/2) + \sin^2(\theta/2)}\right]. \tag{2}$$

This formula can be used directly in the Monte Carlo for single scattering. For initial and final momenta and spin vectors represented by $(\vec{p}_i, \hat{\zeta}_i)$ and $(\vec{p}_f, \hat{\zeta}_f)$, respectively, $\zeta_{f,f} = P'$, the component of $\hat{\zeta}_f$ along $\vec{p}_f$, after a single

scattering through angle θ, is readily obtained by evaluating Eq. 2. To obtain the remaining two $\hat{\zeta_f}$ components a coordinate system $(\hat{n}, \hat{b}, \hat{p}_f)$ is used where $\hat{n} = \hat{p}_i \times \hat{p}_f$ and $\hat{b}$ completes a right handed system. The spin component along $\hat{n}$, perpendicular to the scattering plane, remains unchanged during scattering: $\zeta_{f,n} = \zeta_{i,n}$. The magnitude of $\zeta_{f,b}$ is determined from normalization of $\hat{p}_f$, while its sign will generally be that of $\zeta_{i,b}$. To be more precise, from Ref. [6] and the small angle approximation

$$\zeta_{f,b} = \zeta_{i,b}\left(1 + \frac{p^2\theta^2}{2\varepsilon^2}\right) - \left(1 - \frac{m}{\varepsilon}\right)\theta P \tag{3}$$

and this should be accurate enough to determine the *sign* of $\zeta_{f,b}$.

The above algorithm is applied to scattering off nuclei above the threshold angle. Muon-electron encounters in which the electron is liberated from the atom result in much smaller angles [7] and the accompanying depolarization is incorporated in the multiple scattering.

2.2.2 Multiple Scattering

For multiple scattering the change in polarization is a product of a large number of factors as appear within the square brackets of Eq. 2. To second order in θ this product becomes

$$P' = P\left(1 - \sum \theta_j^2/2\gamma^2\right). \tag{4}$$

Third order terms have zero expectation and higher orders are neglected because of the smaller angles involved. The scattering algorithm deals with *projected* angles: $\sum \theta_{j,x}^2 + \theta_{j,y}^2 = \sum \theta_j^2$. The average of $\sum \theta_{j,x}^2$ may be written as $n\langle\theta_x^2\rangle$, where the j-subscript is omitted in dealing with an individual event, and n is the number of scatterings.

For the individual scattering law assumed in [4]

$$W(\theta_x) = \frac{\theta_0^2(\theta_c^2 + \theta_0^2)^{1/2}}{2\theta_c(\theta_x^2 + \theta_0^2)^{3/2}}, \tag{5}$$

where θ_0 is a constant associated with screening of the nuclear charge by atomic electrons, one obtains

$$\langle\theta_x^2\rangle = \frac{\theta_0^2(\theta_c^2 + \theta_0^2)^{1/2}}{2\theta_c}\log\left(\frac{(\theta_c^2 + \theta_0^2)^{1/2} + \theta_c}{(\theta_c^2 + \theta_0^2)^{1/2} - \theta_c}\right) - \theta_0^2 \tag{6}$$

where θ_c is the threshold projected angle. The distribution of $\sum \theta_{j,x}^2$ about $n\langle\theta_x^2\rangle$ is assumed to be Gaussian with variance equal to $n(\langle\theta_x^4\rangle - \langle\theta_x^2\rangle^2)$ where $\langle\theta_x^4\rangle$ may be found from Eq. 5 as well [8]:

$$\langle\theta_x^4\rangle = \frac{\theta_0^2(\theta_c^2+3\theta_0^2)}{2} - \frac{3\theta_0^4(\theta_c^2+\theta_0^2)^{1/2}}{4\theta_c}\log\left(\frac{(\theta_c^2+\theta_0^2)^{1/2}+\theta_c}{(\theta_c^2+\theta_0^2)^{1/2}-\theta_c}\right). \quad (7)$$

The above equations do not take into account fluctuations in the number of encounters in a Monte Carlo step, n, about its average, $\bar{n}$. For thin targets this fluctuation may become significant and it is therefore routinely included here by choosing n from a Gaussian with parameters $(\bar{n}, \sqrt{\bar{n}})$.

For samples chosen from a normal distribution, the *sample* mean and variance are independent [9]. The sample under consideration here is the number of events in a Monte Carlo step and the variable is the projected angle θ_x for which the sample mean is $\langle\theta_x\rangle = \Theta_x/n = \sum\theta_{j,x}/n$, with sample variance $\sigma_{\theta,x}^2 = \sum\theta_{j,x}^2 - \Theta_x^2/n$. For a sufficiently large sample, one might expect approximate independence even if the variance is calculated with respect to the *population* mean, $\overline{\theta}(=0)$, since the sample mean converges to this value. While the underlying population, viz., Eq. 5, is far from normal one might expect mean and variance to become approximately independent when the distribution of Θ_x, the x-projected scattering angle randomly chosen in a step, approaches the normal. This is the basis of the Gaussian approximation to multiple scattering—although corrections to it are deemed necessary: Edgeworth series and large angle cut-off. With identical reasoning for θ_y it follows that scattering angle and polarization are independent when limited to sufficiently small angles, i.e., limited cut-off angle, and when Monte Carlo step size is large enough. Thus the strategy of treating a few large angle scatterings individually and the rest collectively should work for polarization as well.

It is interesting to put all this to a test and display an example of the correlation between depolarization—proportional to $\sum\theta_{j,x}^2+\theta_{j,y}^2$—and scattering angle (squared) $\Theta^2 = (\sum\theta_{j,x})^2 + (\sum\theta_{j,y})^2$ as might be observed in a typical Monte Carlo step. Fig. 1 shows three scatterplots relating the above variables at the end of a 0.5 cm thick liquid hydrogen target upon which muons of 0.1 GeV/c are incident. The 0.5 cm target thickness might correspond to a typical step in the simulation. Each point in each of the three graphs represent a series of scattering events below a chosen threshold angle—indicated by N, the number of collisions left to be treated individually in that step, with $N = 0$ indicating the absence of a threshold. There are no shortcuts and no collective treatments in Fig. 1: muons are tracked

through the target using the scattering law Eq. 5 (with appropriate cut-off) to simulate each collision individually, i.e., it shows what a collective treatment should strive to match. It is shown in [10] that—independent of target thickness, material, or particle energy—N is a good parameter to separate collective from individual behavior when studying energy loss. It can serve equally well in the treatment of multiple scattering [4]. Superimposed on the plots is a linear least square fit of the *average* of $\sum \theta_{j,x}^2 + \theta_{j,y}^2$ *versus* $(\sum \theta_{j,x})^2 + (\sum \theta_{j,y})^2$. The $N = 0$ plot (top) shows relatively strong correlations and a highly non-Gaussian distribution for $\sum \theta_{j,x}^2 + \theta_{j,y}^2$ at any value of $(\sum \theta_{j,x})^2 + (\sum \theta_{j,y})^2$. The lower two plots show both these unwanted behaviors to decline rapidly with increasing N—even though they do not disappear completely. As the middle graph of Fig. 1 shows, $N = 1$ or perhaps a bit higher, offers a good choice of cut-off angle insofar as correlations are almost absent: about 10% over the extent of the graph, but much less where there is a significant muon population. Incidentally, whereas the Moliere distribution does a good job of representing thick target angular distributions, e.g., the marginal distribution with respect to the abcissa of the $N = 0$ case in Fig. 1, it has nothing to say about correlations.

Figs. 2–4 contrast correlations, again between $\sum \theta_{j,x}^2 + \theta_{j,y}^2$ and $(\sum \theta_{j,x})^2 + (\sum \theta_{j,y})^2$, obtained with the Gaussian approximation as opposed to event-by-event simulation for three beryllium targets of thickness 0.01, 0.1 and 1 cm, respectively. The cut-off angle, θ_c, is chosen to correspond to a value of N=2, i.e., *two* events remain to be simulated individually in Monte Carlo steps of either 0.01, 0.1, or 1 cm. In each figure the *top* part is obtained by simulating *all events below* θ_c individually while in the *bottom* part $\sum \theta_{j,x}^2 + \theta_{j,y}^2$ is chosen from a Gaussian distribution independent of the scattering angle (abcissa). The comparisons shows that for N=2 the Gaussian approximation with parameters as per Eqs. 6 and 7 (without correlation) appears indeed quite adequate when studying polarization associated with small angle multiple scattering.

Based on these considerations, the algorithm adopted for *multiple* scattering in a Monte Carlo step, which includes changes in polarization, is:

(i) Choose a number of collisions, n, from a Gaussian with parameters $(\bar{n}, \sqrt{\bar{n}})$.
(ii) Select an angle $\Theta_x = \sum \theta_{j,x}$ from the Edgeworth series as outlined in [4].
(iii) Choose $\sum \theta_{j,x}^2$ from a Gaussian $(n\langle\theta_x^2\rangle, \sqrt{n(\langle\theta_x^4\rangle - \langle\theta_x^2\rangle^2)})$.
(iv) Repeat steps (ii) and (iii) for the y-projected angles.
(v) Determine the new momentum from the scattering angle $\Theta = (\Theta_x^2 + \Theta_y^2)^{1/2}$ and random azimuthal angle.

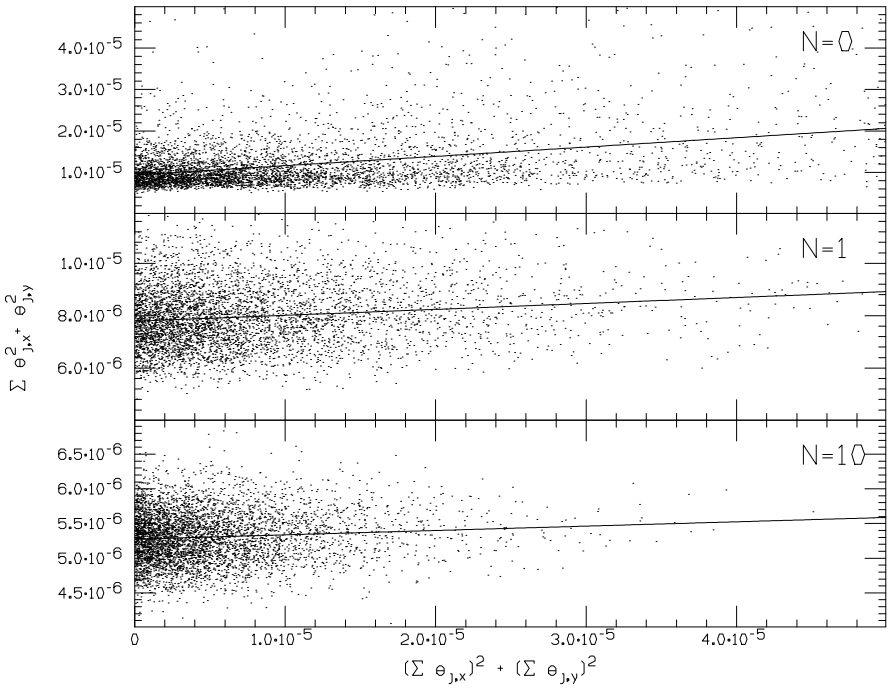

Figure 1: Correlation between $\sum \theta_{j,x}^2 + \theta_{j,y}^2$ (polarization) and $(\sum \theta_{j,x})^2 + (\sum \theta_{j,y})^2$ (scattering angle) for liquid hydrogen target of 0.5 *cm* thickness, as obtained by complete simulation of individual events, for three angular cut-offs expressed as the number of events, N, which remain to be simulated individually.

(vi) Determine the new polarization: $P' = P[1 - (\sum \theta_x^2 + \sum \theta_y^2)/2\gamma^2]$ which yields the component of $\hat{\zeta}$ along $\vec{p}_f$.
(vii) Assign *random* orientation to the component of $\hat{\zeta}$ in the plane perpendicular to $\vec{p}_f$.

Step (vii) assumes that the full range of azimuthal angles is explored over the many encounters treated collectively in each Monte Carlo step. The *angles* associated with μe^--processes are incorporated in the algorithm as outlined in [4]. Their contribution to *depolarization* is included in step (iii) by replacing Z^2 by $Z(Z+1)$ to evaluate the number of encounters in step (i). The effect of μe^--encounters with electron recoil on the polarization is expected to be small and is not separately evaluated.

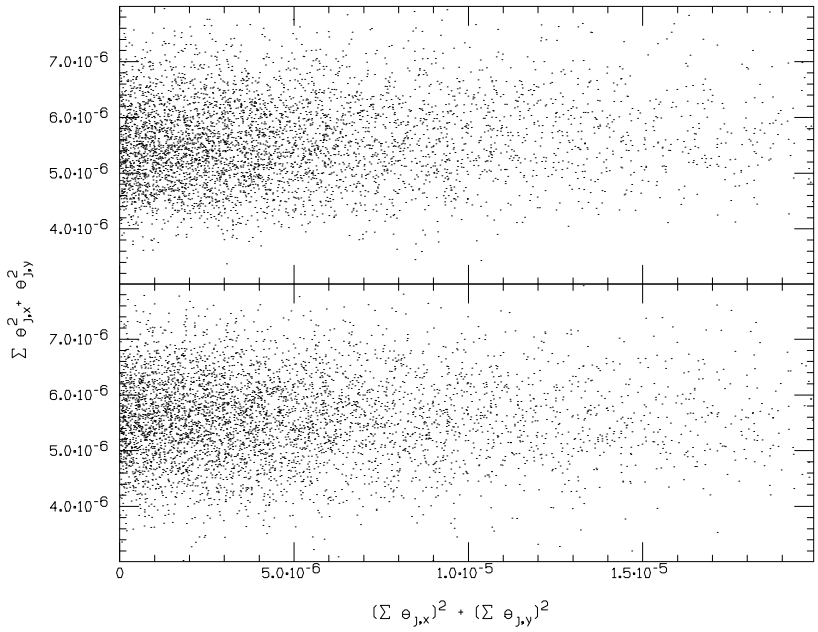

Figure 2: Correlation between $\sum \theta_{j,x}^2 + \theta_{j,y}^2$ and $(\sum \theta_{j,x})^2 + (\sum \theta_{j,y})^2$ for beryllium target of 0.01 g/cm^2 thickness, as obtained by complete simulation of individual events **(top)** and with algorithm **(bottom)**.

3 Results

First some results are presented for absorbers only and compared with analytic formulae followed by results for a cooling channel example.

3.1 Absorbers Only

Results obtained with SIMUCOOL for typical cooling channel absorbers are presented. Average depolarization can also be calculated approximately by analytical methods and is included here mainly to provide a check on SIMUCOOL.

3.1.1 SIMUCOOL

On the basis of the single scattering depolarization formulae one expects some correlation to exist between helicity and $p_\perp$ after transport through an absorber. In SIMUCOOL, such correlations arise strictly from the scatterings which are simulated individually since they are ignored in the collective

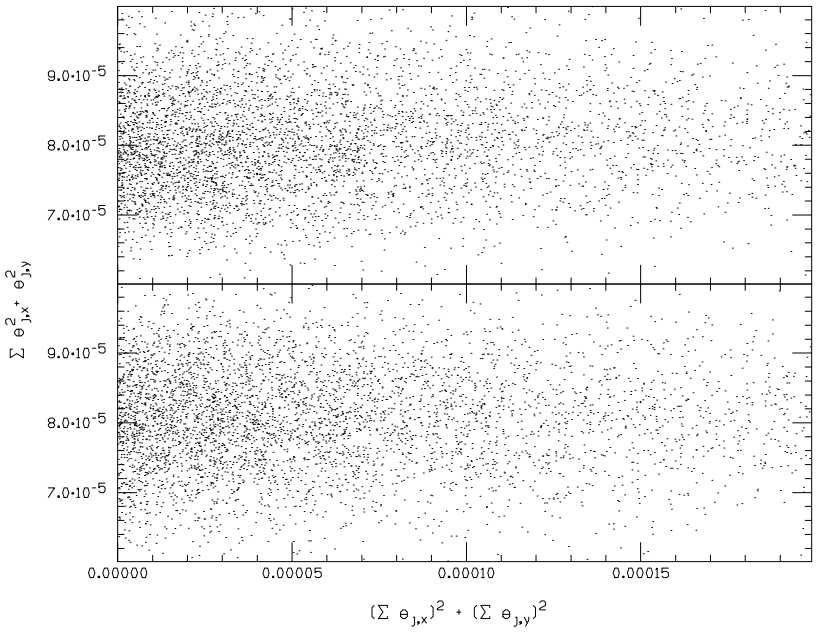

Figure 3: Same as Fig. 2 but for target of 0.10 g/cm^2 thickness.

regime—quite properly as argued above and demonstrated in Figs. 2–4. (For very thick targets, when $\langle\theta^2\rangle^{1/2} \geq \theta_{max}$ and the collective regime reigns throughout, one could expect the correlations to disappear altogether, but these thicknesses are too large to be of practical use in the present problem.)

Fig. 5 presents a suite of scatterplots displaying $p_\perp$ *versus* helicity at various depths when a muon beam with $p_{z,0}$=0.2 GeV/c, $p_{\perp,0}$=0 and with initial helicity $h_0 = 1$, penetrates a 2 m long liquid hydrogen target. Correlations between h and $p_\perp$ are clearly present although, with increasing depth, the more strongly correlated points tend to fall outside the domain of Fig. 5. Fig. 6 plots energy—measured from the average energy—*vs* helicity for the same beam, target thicknesses, and depolarization formula. Since energy loss is predominantly the result of muon-electron encounters while depolarization arises mainly from muon-nuclear scattering there is, as expected, little correlation between the two. Second order effects such as, e.g., longer pathlengths, which cause both energy loss and depolarization to increase, might result in the correlation observed between the upper limit of $h - h_0$ and energy. In Fig. 7 a set of $p_\perp$ *versus* helicity plots—similar to Fig. 5—is presented for 0.2 GeV/c muons traversing a 20 cm thick beryllium target. Fig. 8 shows the same results as fig. 7 but over a much larger helicity

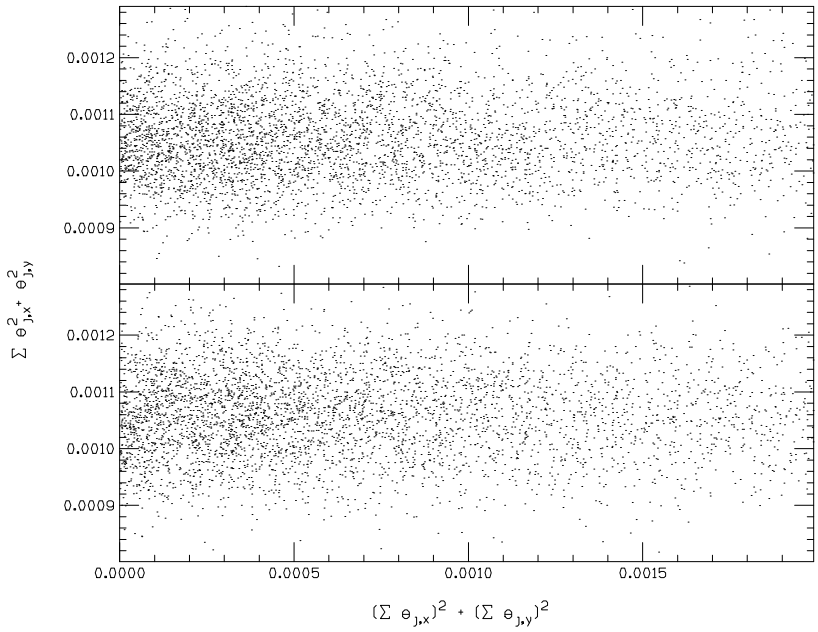

Figure 4: Same as Fig. 2 but for target of 1.00 g/cm^2 thickness.

range. It is based on $5 \cdot 10^5$ incident muons to increase statistics of events with high depolarization.

3.1.2 Average Depolarization

Average depolarization as a function of depth can be estimated analytically starting from the depolarization formulae for single scattering. [7] These provide an important check on SIMUCOOL calculations. The treatment here differs from [7] mainly in that the muon energy loss—which occurs simultaneously with depolarization and at a much faster rate—is included, as well as in a few lesser details. For an infinitesimal target, of thickness dz, the (average) depolarization can be written as

$$dP = \bar{n}\langle \delta P \rangle \, dz \tag{8}$$

where $\langle \delta P \rangle$ is the average depolarization in a single collision and $\bar{n}$ is the average number of collision per unit length. For the individual scattering law, expressed as a function of polar angle, θ,

$$W(\theta) = \frac{2\theta_0^2 \theta}{(\theta_0^2 + \theta^2)^2} \tag{9}$$

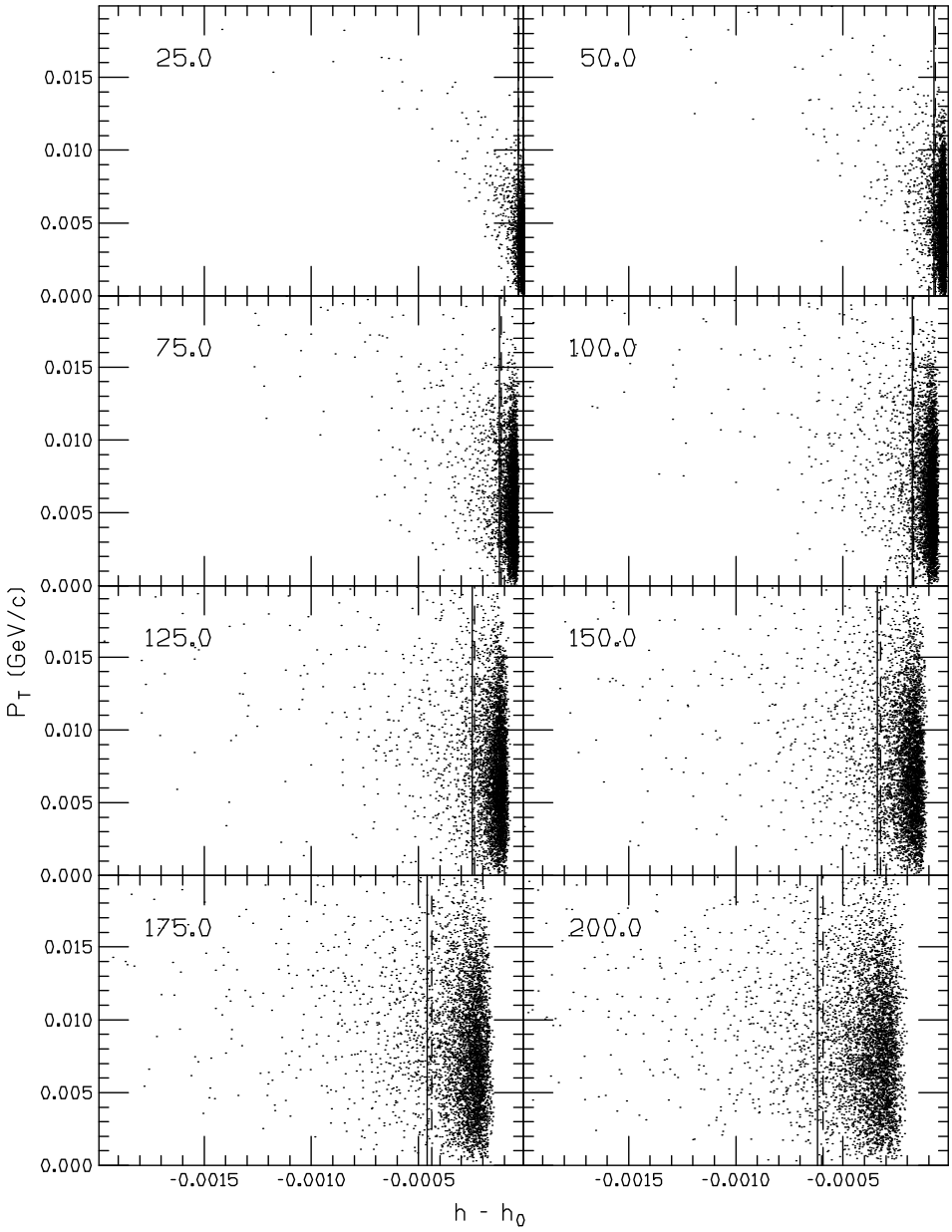

Figure 5: Correlation between depolarization and $p_\perp$ for muon beam with $p_{z,0}$=0.2 GeV/c, $p_{\perp,0}$=0 and h_0=1 at various depths (cm) in liquid *hydrogen* target. Solid vertical line is *average* depolarization as predicted by SIMUCOOL, dashed vertical as per Eq. 12.

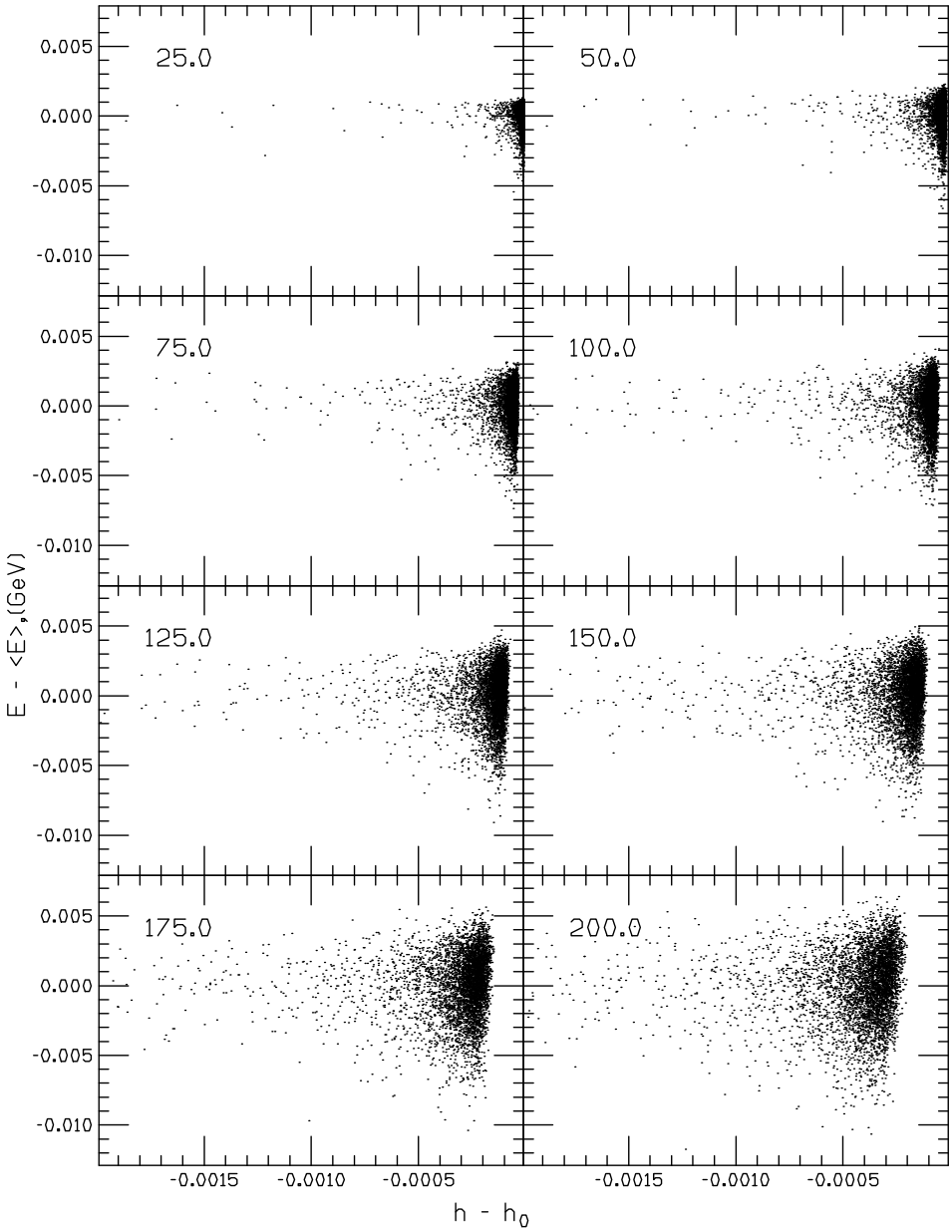

Figure 6: Correlation between depolarization and *energy* for muon beam with $p_{z,0}$=0.2 GeV/c, $p_{\perp,0}$=0 and h_0=1 at various depths (cm) in liquid *hydrogen* target. Solid vertical line is *average* depolarization as predicted by SIMUCOOL, dashed vertical as per Eq. 12.

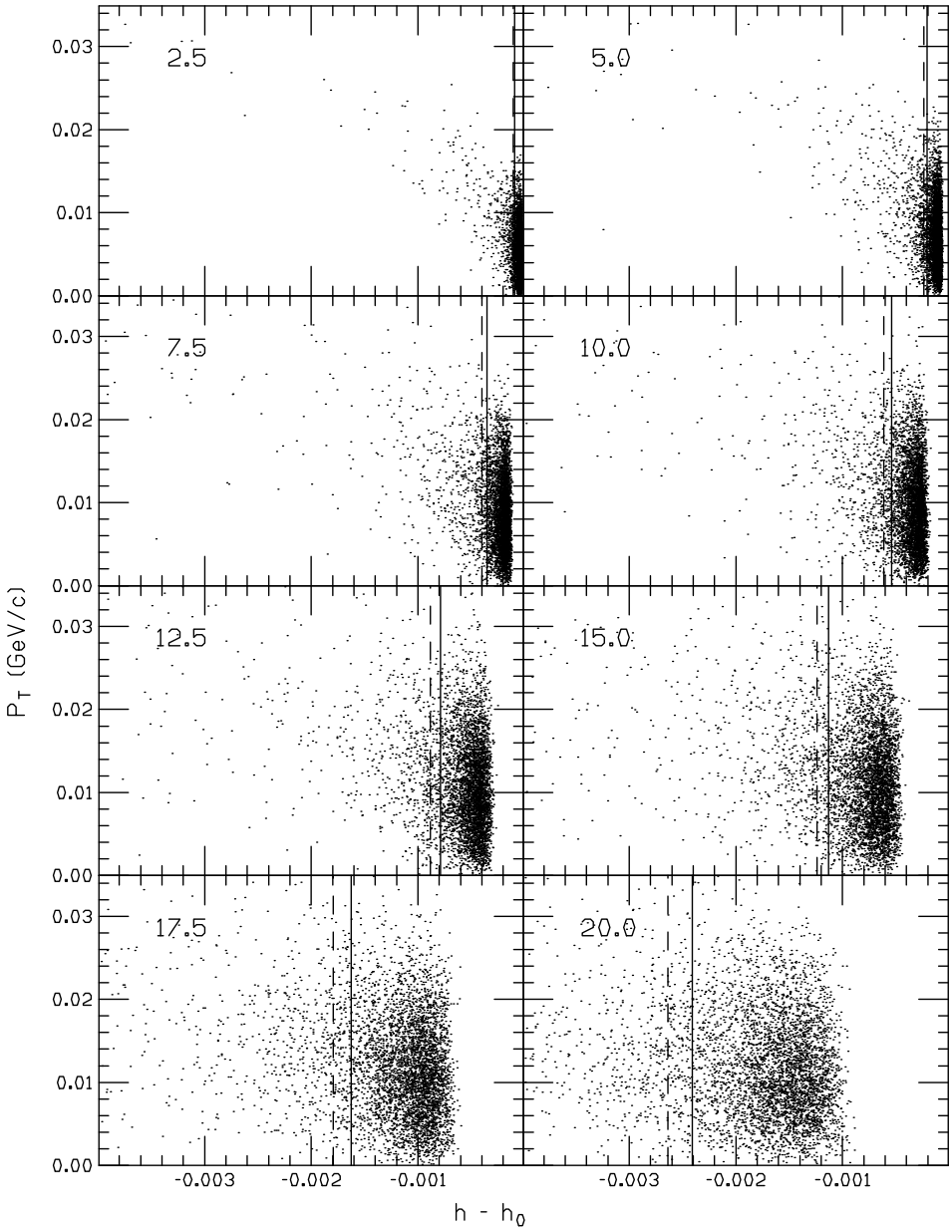

Figure 7: Correlation between depolarization and $p_\perp$ for muon beam with $p_{z,0}$=0.2 GeV/c, $p_{\perp,0}$=0 and h_0=1 at various depths (cm) in *beryllium* target. Solid vertical line is *average* depolarization as predicted by SIMUCOOL, dashed vertical as per Eq. 12.

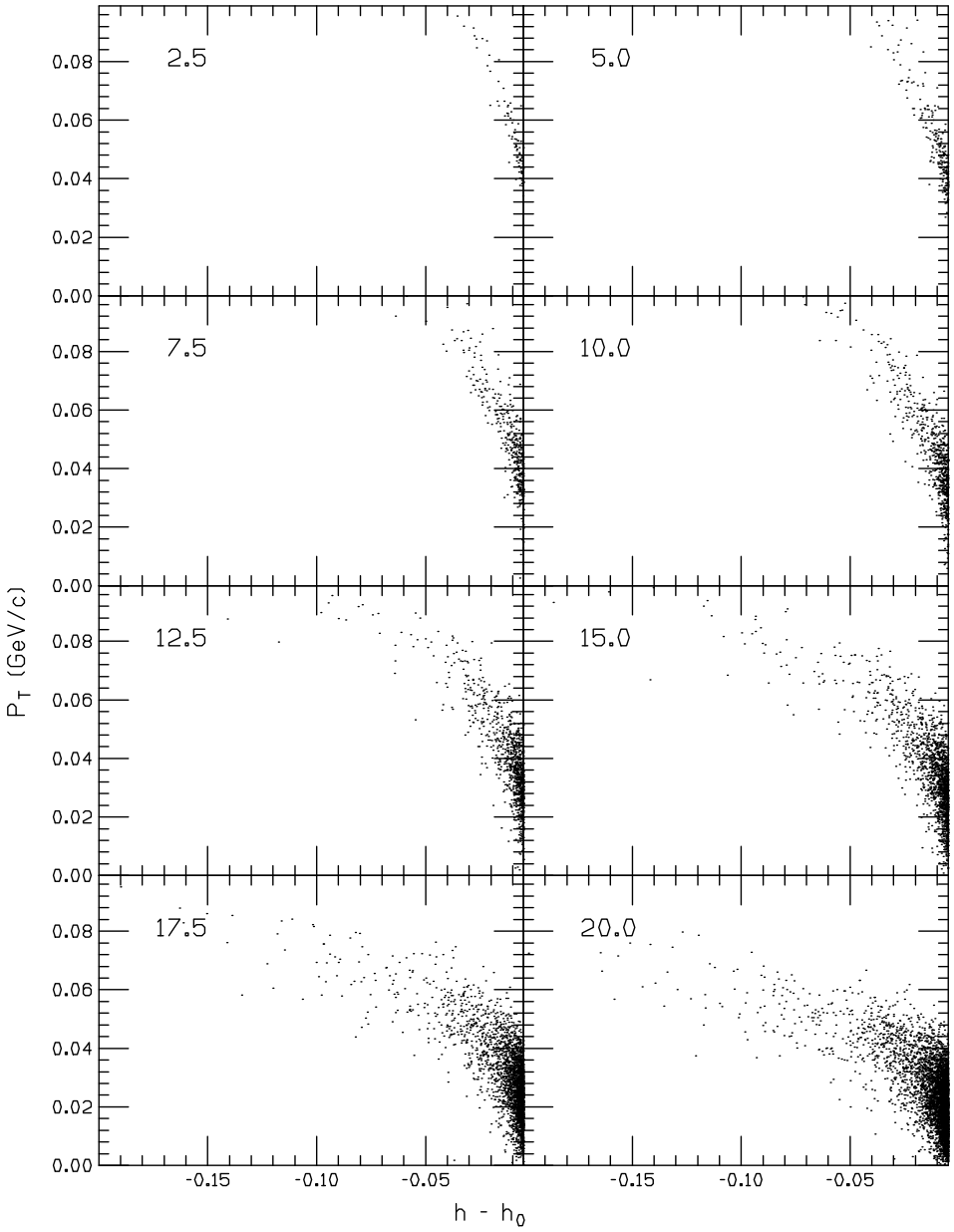

Figure 8: Correlation between depolarization and $p_\perp$ for muon beam with $p_{z,0}$=0.2 GeV/c, $p_{\perp,0}$=0 and h_0=1 at various depths (cm) in *beryllium* target. Plot represents same results as Fig. 7 but with axes rescaled, larger sample of incident muons and with region $h - h_0 > -0.005$ excluded.

and depolarization as per eq. 2 in the small angle approximation

$$\begin{aligned}\langle \delta P \rangle &= P \int_0^{\theta_{max}} W(\theta) \frac{1}{2\gamma^2} \theta^2 d\theta \\ &= P \frac{\theta_0^2}{\gamma^2} \left[\log \frac{\theta_{max}}{\theta_0} - \frac{1}{2} \right] \end{aligned} \tag{10}$$

while $\bar{n} = 4\pi N_{Av} e^4 \left[Z(Z+1)\rho/A \right] \left(\varepsilon^2 / p^4 \theta_0^2 \right)$. In Eq. 10, θ_{max} is associated with nuclear size [11] and has the value $274 m_e / A^{1/3} p$. To include the (average) energy loss, the simplified law

$$\left(\frac{dE}{dx} \right) = \left(\frac{dE}{dx} \right)_0 \frac{1}{\beta^2} \tag{11}$$

is assumed where $\left(\frac{dE}{dx} \right)_0$ is the minimum ionizing stopping power. This should hold fairly well in the energy regime of interest to muon cooling. Eq. 8 must now be integrated over finite thickness, Δz, and this is facilitated by switching to average total energy, ε, as the independent variable:

$$\begin{aligned}\Delta P &= 4P\pi N_{Av} e^4 \left[\frac{Z(Z+1)\rho}{A} \right] \left[\log \frac{\theta_{max}}{\theta_0} - \frac{1}{2} \right] \left| \frac{dE}{dx} \right|_0^{-1} \int_{\varepsilon_1}^{\varepsilon_0} \frac{m^2}{\varepsilon^2 p^2} \, d\varepsilon \\ &= 4P\pi N_{Av} e^4 \left[\frac{Z(Z+1)\rho}{A} \right] \left[\log \frac{\theta_{max}}{\theta_0} - \frac{1}{2} \right] \left| \frac{dE}{dx} \right|_0^{-1} \\ &\quad \times \left[\frac{1}{\varepsilon_0} - \frac{1}{\varepsilon_1} - \frac{1}{m} \log \frac{(m+\varepsilon_0) p_1}{(m+\varepsilon_1) p_0} \right]. \end{aligned} \tag{12}$$

where ε_0 and ε_1 are the average total energy, at the start and end of the absorber, respectively. To evaluate ε_1 one relies on the more accurate dE/dx formula, see e.g. Ref. [12], rather than Eq. 11.

Predictions of these analytical formulae along with the average depolarization obtained from the SIMUCOOL simulation are shown in Figs. 5 and 7 as vertical lines: solid for SIMUCOOL, dashed for the analytical formulae. The position of the average *vs* that of the bulk of the population clearly shows the influence exerted on the average by relatively few large depolarizing scatterings. More precise comparisons of the average results of Fig. 7 are presented in Table 1.

There are a number of differences between the analytical treatment and SIMUCOOL, perhaps the most important one being the sharp cutoff at θ_{max} in Eq. 12 *versus* the use of form factors in the simulation. Given these differences, and the strong influence of the tails on the average, disagreement at the 10–15% level, as observed for the beryllium target, is not surprising.

Table 1: Comparison of SIMUCOOL with analytic calculation of average depolarization *versus* depth in *cm* for muons with p_z=0.2 GeV/c, $p_\perp$=0 and $h_0 = 1$ traversing a beryllium target.

Z,cm	SIMUCOOL	Eq.12	Z,cm	SIMUCOOL	Eq.12
2.5	0.000092	0.000107	12.5	0.000787	0.000884
5.0	0.000207	0.000238	15.0	0.001129	0.001238
7.5	0.000351	0.000402	17.5	0.001626	0.001795
10.0	0.000538	0.000611	20.0	0.002407	0.002638

To determine accurately the average depolarization in SIMUCOOL requires a rather large sample of muon traversals to be simulated so as to explore the large angle regime adequately. Table 1 and the SIMUCOOL average indicated in Fig. 7 are based on $2.5{\cdot}10^6$ muons, while the average of Fig. 5 is based on 10^5 muons. For clarity, only limited numbers are shown in the scatterplots.

3.2 Cooling Channel

In simulating the cooling channel it is advantageous to track the entire set of muons under consideration from cavity to cavity [13]. This allows the phase of each cavity to be optimized based on energy and arrival time of each muon of the sample being studied. A simple optimization strategy is adopted: when a muon arrives at a cavity it is determined what the phase of the cavity should be in order to restore—as best as possible—the muon's energy to the central energy in a single traversal. After all muons have arrived at the cavity the phase adopted is the average over the restoring phases calculated in this manner. Using the RF phase thus optimized, the entire set is then transported through the cavity, the following solenoid and absorber, and then on to the next cavity where the process is repeated. More sophisticated strategies may improve yield and could also aim at limiting depolarization.

Table 2 presents results for average helicity changes when a muon beam travels down a cooling channel approximately 145 m long. A monochromatic muon beam starts out with initial longitudinal momentum, $p_{z,0}$, of either 0.15, 0.25 or 0.4 GeV/c and with initial transverse momentum, $p_{\perp,0}$, of either 0 or 0.125 GeV/c. The channel is equipped with 50 absorbers of liquid hydrogen each 40 cm long. There are an equal number of 200 MHz RF cavities which restore the average energy loss incurred in the absorbers. A 5 Tesla solenoidal field is assumed to apply over the entire length of the chan-

Table 2: Number of muons per proton and average helicity at end of *cooling channel* as a function of initial h_0, $p_{\perp,0}$, and $p_{z,0}$.

$p_{z,0}$	$p_{\perp,0}$	μ/p	Lost	$\langle h \rangle$		
GeV/c				h_0=0	0.50	1.00
0.15	0.000	0.088	0.805	-0.0001	0.4953	0.9908
0.25	0.000	0.894	0.015	0.0001	0.4995	0.9990
0.25	0.125	0.671	0.240	-0.0003	0.4990	0.9984
0.40	0.000	0.894	0.019	0.0000	0.4999	0.9999

nel. In between absorbers and cavities are 1.25 m long gaps where only the magnetic field is present. Absorbers and cavities occupy the full aperture. Muons are no longer followed if they exceed the aperture radius of 20 cm. The above parameters, while not specific to any design, are representative of those used in a number of cooling channel studies and polarization changes are not expected to be very sensitive to the particular values adopted. Initial helicity, h_0, as listed in Table 2, is the same for each beam particle. The choice of a fixed helicity—rather than a broad, momentum-correlated spectrum emanating from the decay channel—is intended to sharpen the depolarization results.

Results of Table 2 are based on samples of 10000 muons for $p_{z,0}$=0.25 and 0.40 GeV/c but is increased to 40000 for $p_{z,0}$=0.15 GeV/c to compensate for the large losses which compromise statistical accuracy of the surviving sample. Results pertain to *all* muons reaching the end of the channel but do not change much when broad cuts are made in the time-energy plane. As expected from the basic depolarization formulae, starting with opposite sign helicity, $-h_0$, results in a final polarization of $-\langle h \rangle$. For initial conditions as in Table 2, column 3 shows muons per proton at the end of the channel, while column 4 lists the fraction of muons lost by exceeding the aperture with the missing muons lost by decay. Results show depolarization over the entire channel to be very small and that larger depolarization occurs at lower $p_{z,0}$—not surprisingly in view of the larger scattering angles expected there. Where aperture losses are significant, increasing the aperture will lower $\langle h \rangle$ since $p_\perp$–h correlations cause muons with higher h to be lost preferentially. Selective removal of the high $p_\perp$ particles is the main reason why the depolarization exhibited in Table 2 remains small even at the lower energies. Note that according to Eq. 2 the absolute value of the helicity always decreases in an absorber whereas in a cavity $|h|$ may go up

as well as down. From the basic formulae one expects the change in helicity in both absorbers and cavities to be proportional to the (initial) helicity which explains the approximate constancy of $\langle h \rangle / h_0$ observed across each row in Table 2. Comparison between the two $p_z = 0.25$ GeV/c cases shows some dependence on $p_{\perp,0}$ most likely resulting from second order effects of increased pathlength in the absorber, differences in average cavity field encountered due to different transit times, etc.

To examine the effects on polarization of the absorbers *versus* that of the cavities, polarization changes in the latter are 'turned off', i.e., upon exiting a cavity with a new momentum, the helicity is restored to its entrance value while the other spin components are renormalized. For $p_\perp$=0, final helicities are practically identical with those of Table 2 whereas at larger $p_{\perp,0}$ the difference with Table 2 increases with h_0. Thus, in Table 2 only the third row is affected ($p_{z,0}$=0.25 GeV/c, $p_{\perp,0}$=0.125 GeV/c). The largest change occurs for h_0=1 where the final $\langle h \rangle$ is now 0.9935. This shows that most of the depolarization is due to the absorbers and that the fields in the cavities *counteract* this depolarization—a direct result of the phase stability provided by the cavities.

4 Concluding Remarks

Division into single and multiple scattering, which already provides a convenient and accurate way to simulate angular dispersion, also works well in the study of polarization. It becomes essential if one wishes to investigate correlations between angles ($p_\perp$) and polarization incurred while traversing a thick target. This relates to the point made by Scott and quoted in the Introduction. Assume a single large scattering event occurs somewhere in a Monte Carlo step with an angle well in excess of the *rms* angle for multiple scattering. Typically, the cumulative angle of that step will then be close to the angle of that one event but cumulative depolarization will be close to proportional to the *square* of that angle. A collective (Gaussian) treatment of multiple scattering typically fails at around 2σ [11] and, as the Scott argument suggests, collective treatment of the polarization fails at even smaller deviations from the mean.

As the examples shown in Table 2 suggest, overall depolarization in a typical cooling channel is very small—at most of order one percent. In many applications it appears that it can either be neglected or that it may suffice to calculate average depolarization. A more definitive conclusion best awaits simulations which include more realistic fields in magnets and cavities.

My thanks to J. D. Bjorken for helpful comments on depolarization and to D. Neuffer for suggestions and corrections regarding the manuscript.

References

[1] A. Van Ginneken, *Polarization of Muons in Decay Channel*, MuCool Note 65 (1999).

[2] A. Van Ginneken, Nucl. Inst. Meth **A362**, 213 (1995); N. V. Mokhov and S. I. Striganov, *Simulation of Backgrounds in Detectors and Energy Deposition in Superconducting Magnets at $\mu^+\mu^-$ Colliders*, in Proc. 9th Advanced ICFA Beam Dynamics Workshop, Montauk, N.Y., Oct. 15–20 (1995).

[3] W. T. Scott, Rev. Mod. Phys. **35**, 231 (1963).

[4] A. Van Ginneken, Nucl. Inst. Meth. **B160**, 460 (2000).

[5] J. D. Bjorken and S. D. Drell, *Relatrivistic Quantum Mechanics*, McGraw Hill, New York (1964).

[6] V. B. Berestetskii, E. M. Lifshitz and L. P. Pitaevskii, *Quantum Electrodynamics. Landau and Lifshitz Course of Theoretical Physics*, Vol. 4, 2nd Ed., p. 320, Pergamon (1982).

[7] R. C. Fernow, J. C. Gallardo, and Y. Fukui, *On Muon Depolarization Effects in an Ionization Cooling Channel*, MuCool Note 115 (2000).

[8] In many instances the condition $\theta_c \gg \theta_0$ applies in which case Eqs. 6 and 7 simplify considerably. However, in the simulation θ_c is dependent upon step length which—e.g., near a material boundary—is not always conveniently at the user's disposal, so that the above condition may not hold universally and such simplifications are avoided at a small expense of some extra computation (since simplification of the angle selection algorithm is somewhat less dramatic than that of the equations).

[9] see, e.g., H. Cramér, Mathematical Methods of Statistics, Princeton Univ. Press (1945).

[10] P. V. Vavilov, Zh. Eksp. Teor. Fiz. **32**, 920 (1957) transl, in Sov. Phys. JETP **5**, 749 (1957).

[11] J. D. Jackson, *Classical Electrodynamics*, 2nd Ed. ,Wiley, New York (1975).

[12] C.Caso et al., Eur. Phys. J. **C3**, 1 (1998).

[13] W. Chou and A. Van Ginneken, *Phase Rotation Using Low Frequency (Few MHz) RF*, MuCool Note 90 (2000).